

Structure in Aqueous Solutions of Nonpolar Solutes from the Standpoint of Scaled-Particle Theory¹

Frank H. Stillinger²

Received October 30, 1972

Underlying assumptions have been examined in scaled-particle theory for the case of a rigid-sphere solute in liquid water. As a result, it has been possible to improve upon Pierotti's corresponding analysis in a way that explicitly incorporates measured surface tensions and radial-distribution functions for pure water. It is pointed out along the way that potential energy nonadditivity should create an orientational bias for molecules in the liquid-vapor interface that is peculiar to water. Some specific conclusions have been drawn about the solvation mode for the nonpolar rigid-sphere solute.

KEY WORDS: Hydrogen bonding; molecular correlation; potential non-additivity; scaled-particle theory; solubility; surface tension; water.

1. INTRODUCTION

The scaled-particle theory of classical fluids offers a powerful conceptual and computational framework within which to examine molecular order and thermodynamic properties. This method was originally devised to describe only the rigid-sphere model without attractive forces.^(1,2) Nevertheless, its scope has since been increased to include models for a wide class of real substances.^(3,4) Furthermore, the underlying theory has been substantially strengthened and deepened in comparison to its early version.⁽⁵⁻⁸⁾

The initial attempts to apply scaled-particle theory to liquid water were disappointing. Both the surface tension and the isothermal compressibility, along the saturation line from 0° to 100°C, were predicted to be too low and to have improper temperature variations.⁽⁹⁾ In view of the strong, directional, and nonadditive interactions that operate in water to produce extensive hydrogen bonding, this failure seems hardly surprising.

¹ This paper is substituted for the talk given at the symposium, "The Physical Chemistry of Aqueous Systems," held at the University of Pittsburgh, Pittsburgh, Pennsylvania, June 12-14, 1972, in honor of the 70th birthday of Professor H. S. Frank.

² Bell Laboratories, Murray Hill, New Jersey 07974.

One of the key quantities in the scaled-particle theory is $W(\lambda)$, the amount of reversible, isothermal work necessary to create a spherical cavity of radius λa in the fluid of interest, whose interior is devoid of molecular centers. Following the usual convention, we use a here to denote a convenient fixed molecular length, and λ varies in the range $0 < \lambda < \infty$. In order for a nonpolar spherical solute molecule to dissolve in a liquid, it must at least have available to it the requisite cavity; as a consequence, $W(\lambda)$ for the appropriate size λa becomes an important contribution to the solubility of that nonpolar solute.⁽¹⁰⁾

Pierotti⁽¹¹⁾ has specifically applied the scaled-particle theory to description of aqueous solutions of nonpolar gases. Somewhat surprisingly, he finds that it is possible to predict heats, entropies, and molar heat capacities of solution merely under the assumption that the water molecules arrange themselves spatially in the pure liquid as would rigid spheres of appropriate size. In view of the current understanding about the interactions between water molecules,⁽¹²⁻¹⁶⁾ this apparent success must be somewhat fortuitous. Certainly, the molecular structure in water revealed by x-ray scattering experiments⁽¹⁷⁾ seems quite different from that appropriate to rigid spheres. It is therefore the purpose of this paper to reexamine one aspect of application of scaled-particle theory to aqueous solutions of spherical, nonpolar solutes, with the aim of restoring chemical detail.

For completeness, Sec. 2 provides an outline of the main ingredients in the scaled-particle theory as well as some numerical results for Pierotti's specific method of application. Section 3 discusses the character of the planar water interface that obtains in the $\lambda \rightarrow \infty$ limit and points out some features of molecular arrangements in the interface that are peculiar to water.

We offer in Sec. 4 a more detailed version of scaled-particle theory for water as a solvent than has heretofore been available. This version incorporates both measured surface tensions and radial-distribution functions for the pure liquid. The results are interpreted in Sec. 5 in a way that accords with the special nature of intermolecular forces in water.

2. PRELIMINARY RESULTS

Consider a set of N molecules confined to the interior of a region with volume V . Thermal equilibrium at absolute temperature T will be assumed. For the moment, at least, no special restrictions need to be imposed about the internal structure of the molecules or about the way in which they interact with one another.

We wish to examine the way that this N -molecule solvent responds to the insertion of a special type of solute particle. This solute particle has the property that it interacts with the solvent molecules only in being unable to get closer than distance λa to the center of each. Thus each solvent molecule has associated with it an exclusion sphere of radius λa , and the center of the

solute particle must forever remain outside of all of these exclusion spheres. Equivalently, solvent molecules are excluded from a sphere of radius λa surrounding the solute particle.

The probability $P(\lambda)$ that a randomly chosen position in the pure solvent lies outside of all exclusion spheres is equal to the fraction of V uncovered by those spheres. This probability can in turn be related⁽¹⁾ to the cavity-creation work $W(\lambda)$ mentioned previously:

$$P(\lambda) = \exp [-W(\lambda)/kT] \quad (1)$$

where k is Boltzmann's constant. If λ is zero, $P = 1$ and $W = 0$; by contrast, $P(\lambda)$ will be very small for large positive λ , and $W(\lambda)$ will be large and positive since many solvent particles would normally have to be moved out of the way to create an uncovered location.

For arbitrary λ , the density of solvent molecule centers, at the surface of the empty radius- λa sphere S_λ surrounding the solute, is traditionally denoted by $\rho G(\lambda)$, where

$$\rho = N/V \quad (2)$$

By considering the work expended during increase of the solute size from 0 to λa , it may be shown⁽¹⁾ that

$$W(\lambda)/kT = 4\pi\rho a^3 \int_0^\lambda (\lambda')^2 G(\lambda') d\lambda' \quad (3)$$

Another fundamental relation in the scaled-particle theory results from expressing $P(\lambda)$, the probability that S_λ is empty, in terms of molecular correlation functions $g^{(n)}$ for molecular centers in the pure solvent. One thus has the following identity:⁽¹⁾

$$P(\lambda) = 1 + \sum_{n=1}^{\infty} [(-\rho)^n / n!] \int_{S_\lambda} d\mathbf{r}_1 \cdots \int_{S_\lambda} d\mathbf{r}_n g^{(n)}(\mathbf{r}_1 \cdots \mathbf{r}_n) \quad (4)$$

The terms in this series will all vanish for orders n exceeding the maximum number of solvent molecule centers that can be packed into sphere S_λ .

Let a be the distance of closest approach of two solvent molecules to each other. Then when $0 < \lambda < \frac{1}{2}$, all terms in (4) beyond $n = 1$ vanish. Since $g^{(1)} \equiv 1$, we then have in this initial λ range

$$\begin{aligned} P(\lambda) &= 1 - (4\pi\rho a^3/3) \lambda^3 \\ W(\lambda)/kT &= -\ln [1 - (4\pi\rho a^3/3) \lambda^3] \\ G(\lambda) &= [1 - (4\pi\rho a^3/3) \lambda^3]^{-1} \end{aligned} \quad (5)$$

As λ begins to exceed $\frac{1}{2}$, two solvent centers can fit into S_λ , so the $n = 2$ term in series (4) begins to contribute. Nevertheless, each of $P(\lambda)$, $W(\lambda)$, and $G(\lambda)$ remain continuous and differentiable at $\lambda = \frac{1}{2}$, and only the last of these three functions can suffer a simple discontinuity in its second λ derivative there.⁽¹⁾

As $\lambda \rightarrow \infty$, $W(\lambda)$ becomes dominated by work against the external pressure p and against the surface tension γ for the cavity-solute interface.³ Thus we have

$$W(\lambda) = (4\pi p a^3/3) \lambda^3 + (4\pi \gamma_\infty a^2) \lambda^2 - (16\pi \gamma_\infty \delta a) \lambda + O(1) \quad (6)$$

here γ_∞ stands for surface tension in the planar interface limit, and δ provides the leading curvature dependence for the mechanical tension γ :⁽¹⁸⁾

$$\gamma \sim \gamma_\infty [1 - (2\delta/\lambda a)] \quad (7)$$

The integral connection (3) between W and G allows us to conclude that the latter has the following large- λ behavior:

$$G(\lambda) = (p/\rho kT) + (2\gamma_\infty/\rho a kT)/\lambda - (4\gamma_\infty \delta/\rho a^2 kT)/\lambda^2 + \dots \quad (8)$$

Insofar as G is concerned, the essence of Pierotti's calculation is to consider the three terms explicitly shown in Eq. (8) to be alone an adequate approximation for all $\lambda > \frac{1}{2}$. The pressure p is chosen according to experimental circumstances, and the solvent contact distance a is assigned the value 2.75 Å (at least below 70°C). The requirement that the $\lambda > \frac{1}{2}$ approximation to G must continuously and differentiably connect to the exact expression (5) at $\lambda = \frac{1}{2}$ then allows one to calculate γ_∞ and δ . The results are the following:

$$\gamma_\infty = \frac{3ykT}{\pi a^2} \left\{ \frac{1}{1-y} + \frac{3}{2} \frac{y}{(1-y)^2} - \frac{p}{\rho kT} \right\} \quad (9)$$

$$\delta = \frac{a}{8} \left\{ 1 + \frac{3y}{2 + y - 2(1-y)^2(p/\rho kT)} \right\} \quad (10)$$

where $y = \pi p a^3 / 6$.

Table I lists some values computed for γ_∞ and δ by Eqs. (9) and (10) at selected points along the saturation curve for water. The table also includes the measured liquid-vapor interfacial tension for comparison, as well as the dimensionless compressibility factors $p/\rho kT$.

Once γ_∞ and δ have been evaluated, $G(\lambda)$ may then be obtained. Figure 1 shows the resulting $G(\lambda)$ at 25°C (and the corresponding pressure for the vaporization curve). Its most distinctive feature is the maximum at $\lambda a = 2.009$ Å. Similar maxima occur for other temperatures, always at

$$(\lambda a)_{\max} = 4\delta \quad (11)$$

in this Pierotti approximation. Evidently the predicted G 's are rather insensitive to temperature below 100°C.

The most significant point to realize about this approximation for $G(\lambda)$ is that the only explicit information it requires about the molecular structure of water is a , the distance of closest approach. Thus water could as well as

³ The Gibbs dividing surface for which γ is appropriate is the geometric surface of S_λ .

Table I. Surface Tension (γ_∞) and Curvature Parameter (δ) Calculated for Liquid Water at Its Saturated Vapor Pressure^a Using the Pierotti Approximation^b

t (°C)	ρ (10^{24} cm $^{-3}$)	p/pkT	γ_{lv} (expt) (dyn·cm $^{-1}$)	γ_∞ [Eq. (2.9)] (dyn·cm $^{-1}$)	δ [Eq. (2.10)] (Å)
4	0.033443	6.3533×10^{-6}	75.07	51.44	0.5026
25	0.033346	2.3068×10^{-5}	72.01	54.97	0.5022
50	0.033043	8.3683×10^{-5}	67.93	58.35	0.5010
75	0.032599	2.4606×10^{-4}	63.49	60.96	0.4992
100	0.032043	6.1391×10^{-4}	58.78	62.86	0.4970
200	0.028917	8.2325×10^{-3}	37.81	63.82	0.4845
300	0.023818	4.5597×10^{-2}	14.39	52.18	0.4648

^a Measured values for ρ , p , and γ_{lv} have been taken from E. Schmidt, *Properties of Water and Steam in SI Units* (Springer-Verlag, New York, 1969).

^b The molecular size a has been assumed to remain constant at 2.75 Å.

not have consisted of rigid spheres (with long-range attractive forces to stabilize the liquid), and no interaction anisotropy.

The shape of the $G(\lambda)$ curve is intimately related to the occurrence of "contact pairs" of solvent molecules at the solute's exclusion cavity S_λ . As Fig. 2 shows, we consider two infinitesimal volume elements dv_1 and dv_2 in contact with (but exterior to) the exclusion sphere and separated by angle θ measured from the center of that sphere. The probability that both dv_1 and dv_2 are simultaneously occupied by solvent molecule centers then may be written

$$\rho^2 G^{(2)}(\lambda, \lambda, \theta) dv_1 dv_2 \quad (12)$$

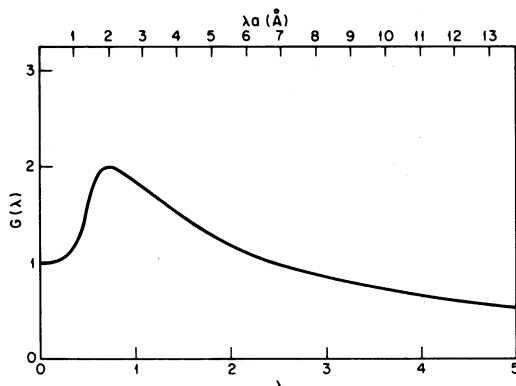


Fig. 1. $G(\lambda)$ for liquid water, calculated in the Pierotti approximation. The temperature is 25°C, and the pressure is that of the vapor-pressure curve. The maximum occurs at $\lambda a = 2.009$ Å.

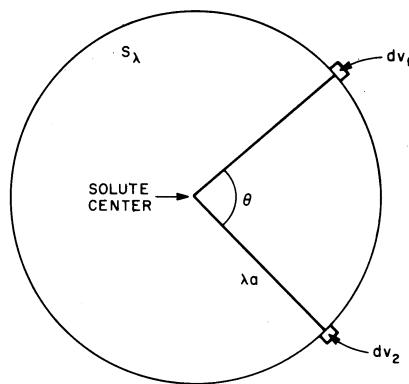


Fig. 2. Arrangement of differential volume elements dv_1 and dv_2 on the solute exclusion sphere, used in definition of the contact-pair correlation function $G^{(2)}(\lambda, \lambda, \theta)$.

thereby introducing a contact-pair analog $G^{(2)}$ of the singlet quantity G . For very large λ and nonzero θ , we naturally expect to have the reduction

$$G^{(2)}(\lambda, \lambda, \theta) \sim [G(\lambda)]^2 \quad (13)$$

that results from statistical independence of dv_1 and dv_2 .

A general relationship has been derived⁽⁷⁾ which links G and $G^{(2)}$:

$$\frac{\partial G(\lambda)}{\partial \lambda} = -2\pi\rho a^3 \lambda^2 \int_0^\pi d\theta \sin \theta (1 - \cos \theta) \{G^{(2)}(\lambda, \lambda, \theta) - [G(\lambda)]^2\} \quad (14)$$

Thus the rate of change of G with λ depends specifically on the deviations of $G^{(2)}$ from the asymptote (13); those deviations in turn sensitively reflect the arrangement patterns preferred by solvent molecules around the solute.

When $0 < \lambda < \frac{1}{2}$, at most one solvent molecule can be in contact with S_λ , so $G^{(2)}$ must vanish for all angles θ . Equation (2.14) then reduces to

$$\frac{\partial G(\lambda)}{\partial \lambda} = 4\pi\rho a^3 \lambda^2 [G(\lambda)]^2 \quad (0 < \lambda < \frac{1}{2}) \quad (15)$$

One easily verifies that the last expression in (5) satisfies this differential equation.

At the maximum in $G(\lambda)$, one must have

$$0 = \int_0^\pi d\theta \sin \theta (1 - \cos \theta) \{G^{(2)}(\lambda_{\max}, \lambda_{\max}, \theta) - [G(\lambda_{\max})]^2\} \quad (16)$$

This identity would seem to be potentially useful in deciding what must be the geometric nature of the solvation sheath for this specific interesting solute size.

The partial molar volume of a solute at infinite dilution, $\bar{v}^{(0)}$, roughly speaking, represents three distinct contributions:

1. The first is the volume increase that would result even for a point particle (not interacting with the solvent molecules) on account of its kinetic contribution to the pressure. The magnitude of this part will be proportional to the pure solvent's isothermal compressibility.

2. The second is just the geometric volume occupied by the solute particle. In the general case, there may be some ambiguity about the precise magnitude of this volume, but for the present model solute it is clearly $\tau(\lambda) = 4\pi a^3 \lambda^3/3$.

3. Finally, one expects that solvent molecule rearrangement to accommodate the solute particle will normally result in a change in packing efficiency for those solvent molecules.⁴ This will also contribute to $\bar{v}^{(0)}$.

It is known⁽⁷⁾ that $\bar{v}^{(0)}$ for our model solute may be written in terms of $G(\lambda)$:

$$\begin{aligned}\bar{v}^{(0)}(\lambda) &= (kT/\rho)(\partial\rho/\partial p)_T + \tau(\lambda) + 4\pi a^3 kT(\partial\rho/\partial p)_T \int_0^\lambda d\lambda' (\lambda')^2 \\ &\quad \times (\partial/\partial\rho)[\rho G(\lambda') - (p/kT)]\end{aligned}\quad (17)$$

The three terms added together in the right member, are respectively, the three contributions (1), (2), and (3) just mentioned.

Entropy provides a fundamental thermodynamic parameter for measuring structure in the solution. From the standpoint of the statistical theory of the present nonpolar solute model, the most revealing comparison occurs between entropy for the pure solvent plus noninteracting point solute (all in volume V) and entropy for the same number of water molecules plus repulsive solute molecule in volume $V + \tau(\lambda)$. With this convention, the volume accessible to the centers of solvent molecules is unchanged, and the resulting entropy variation measures only the result of restructuring around the inserted exclusion sphere. The Helmholtz free energy associated with expansion of the solute sphere (λ increasing from zero to the required final value) and the change in system volume is

$$\Delta_1 A(\lambda) = W(\lambda) - p\tau(\lambda) \quad (18)$$

the corresponding entropy change will be

$$\Delta_1 S = -(\partial W/\partial T)_V + \tau(\lambda)(\partial p/\partial T)_V \quad (19)$$

Ordinarily, solution thermodynamic properties are experimentally observed at constant p . The resulting system volume increment then would be $\bar{v}^{(0)}(\lambda)$ rather than $\tau(\lambda)$. Thus the more conventional solution process quantities are

$$\Delta_2 A(\lambda) = W(\lambda) - p\bar{v}^{(0)}(\lambda) \quad (20)$$

and

$$\Delta_2 S = -(\partial W/\partial T)_V + (\partial p\bar{v}^{(0)})/dT_V \quad (21)$$

For water under ordinary temperature and pressure conditions, the second terms in the right members of Eqs. (19) and (21) are negligibly small, so that solution entropy can be explained satisfactorily in terms of W alone.

⁴ In principle, this phenomenon could be assessed quantitatively by computing the mean Voronoi (nearest-neighbor) polyhedron volume for solvent molecules with and without the solute present.

3. PLANAR INTERFACE

As λ approaches infinity, the surface of S_λ locally takes on the appearance of an impenetrable planar wall, so far as the neighboring water molecules are concerned. We now turn attention specifically to the question of how these water molecules are arranged in the immediate vicinity of this limiting flat wall.

Heretofore we have not had to commit ourselves about the position of the "center" of a water molecule with respect to its nuclear framework. Indeed the general exact results of the preceding section are invariant to the choice of "center" (provided we still have $a > 0$). It is characteristic, furthermore, of the Pierotti approximation that specification of the "center" position is unnecessary. Now, however, we must recognize that it is this "center" which encounters and is repelled by the surface of S_λ .

We thus choose to identify the position of the oxygen nucleus in each water molecule as the "center." This choice is suggested by the periodic arrangement of oxygen nuclei in ice (in contrast to the disorder that characterizes proton positions) and by the fact that the pair-interaction potential between water and the simple solute Ne is nearly spherically symmetric about the oxygen.⁽¹⁹⁾ With this convention, one recognizes that the protons of the water molecules can penetrate S_λ to an extent consistent with the intramolecular bond length ($\approx 1 \text{ \AA}$).

Since there are no forces of attraction between water molecules and the surface of S_λ , we cannot expect that the surrounding liquid will "wet" the surface. This fact is borne out by the small value of the molecular density actually in contact with the flat wall:

$$\rho G(\infty) = \rho(p/pkT) \quad (22)$$

Table I shows that the compressibility factor p/pkT is only about 2×10^{-5} at room temperature, so the contact density is only 2×10^{-5} of that in bulk water. In effect, then, the very large sphere S_λ must be immediately surrounded by a thin film of water vapor.⁵ As one proceeds outward from the S_λ surface toward the interior of the bulk-water phase, the average density must rise (probably monotonically at low temperatures) to ρ , its large-distance limit.

While the external pressure p is at or near the saturated vapor pressure for the given temperature, there is essentially no driving force within the system to eliminate the vapor film surrounding S_λ . The film thus can become rather thick on the molecular scale, and its character can properly be assessed in terms of known facts about bulk water vapor. The zone of transition between low vapor density in the film and high liquid density farther out is therefore determined primarily by the same factors⁽²⁰⁾ that determine the normal liquid-vapor interface structure at that temperature. The surface tension γ_∞ then should be very close to the measured liquid-vapor surface tension γ_{lv} .

⁵ At room temperature, the water-vapor second virial coefficient is negative, so in fact the water molecule density (22) is slightly *less* than that of the saturated vapor.

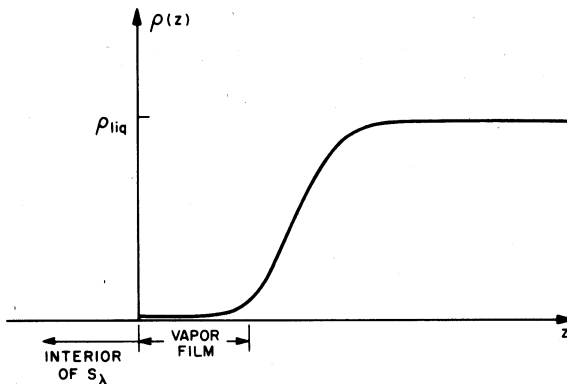


Fig. 3. Water molecule density $\rho(z)$ vs normal distance z from the surface of S_λ . This schematic diagram refers specifically to the $\lambda \rightarrow \infty$ limit for which the impenetrable surface appears locally to be flat. The vapor film results from the nonwettability of the surface.

(some values are listed in Table I). Figure 3 indicates schematically the water-molecule density distribution expected to obtain near the flat boundary.

As the external pressure is isothermally increased, the vapor film will be squeezed out. The pressures required to effect significant changes, though, are rather large in ordinary terms. If the film were to be expelled to the extent that the surface density rose to half that in the bulk water (i.e., $p/\rho kT = \frac{1}{2}$), about 700 bars would be required at 25°C. Small pressure increments above the saturation vapor pressure would mainly have the effect of moving an unperturbed liquid-vapor interface inward, and the γ_∞ that is relevant to the large- λ asymptotic expansion of $G(\lambda)$ [Eq. (8)] remains equal substantially to the measurable interfacial tension γ_{lv} . But at very high external pressures the surface density profile will have been crushed into a totally different form, and the required γ_∞ must come from some other source.

The parameter δ [also appearing in the asymptotic series (8)] has the dimension of length. This length (more precisely 2δ) measures the apparent distance inward from the surface of S_λ at which the surface tension of the spherical interface seems to act mechanically. At very low pressure increments there can be no doubt that -2δ ought to measure the vapor film width. Of course, under extremely large p it is unclear what δ measures; although we expect it to remain comparable to molecular size, even its sign is uncertain.

These considerations cast some doubt on the accuracy of the approximate water calculation outlined in the preceding section. Table I shows that the computed surface tension has the wrong temperature variation. Furthermore, the computed values for δ have the wrong sign and are certainly too small. Though we cannot be certain what its value strictly ought to be, it seems clear that -2δ should be no less than measured interfacial widths. Experiments by Kinoshita and Yokota,⁽²¹⁾ using an ellipsometric technique, suggest that this

width is about 8 Å at 25°C. The Pierotti calculation therefore seems seriously to misrepresent δ near saturation pressure.

Having established that the low-pressure interface next to the flat repelling surface is closely related to the free liquid surface, it is relevant to inquire how water molecules are oriented within both. The preferred orientations depend on the molecular structure and on the nature of water-molecule interactions.

One orienting agency was previously pointed out by Stillinger and Ben-Naim,⁽²²⁾ which stems from the electrical asymmetry of the separate water molecules. The sign of the axial quadrupole moment indicates that the effective position of the molecule's permanent dipole moment is forward of the oxygen nucleus (i.e., toward the bisector of the line connecting the protons). As a result, there is a mean torque on molecules in the interface tending to orient their dipoles toward the bulk liquid. Consequently, the mean electrostatic potential increases upon passage through the interface from the vapor side to the liquid side, since molecules at the surface tend to immerse their protons and expose their lone-pair electrons.

The peculiar character of interaction nonadditivity in water is also capable of biasing the interfacial-region orientational distribution. The predominant nonadditive component to the potential in a water molecule assembly is probably three-molecule nonadditivity, which depends strongly on the hydrogen-bond pattern.⁽¹⁵⁾ Any hydrogen-bond network with perfect fourfold coordination has an invariant number of three types of molecular neighbor trimers:

- (a) Double donor trimer—one molecule simultaneously donating its protons in hydrogen bonds to two other molecules;
- (b) Double acceptor trimer—one molecule simultaneously acting as the acceptor for two protons donated by distinct neighbors;
- (c) Sequential trimer—a central molecule simultaneously accepts a proton from one neighbor and donates one of its own to a second neighbor.

The relative network occurrence frequencies for these three neighbor types are respectively 1:1:4. The three-molecule potential energy nonadditivity $V^{(3)}$ is positive for the first two types but negative for the last type. Figure 4 shows specific examples of each of the three types. For counting purposes in an extended network, these trimers may be regarded as "belonging to" the middle one of the three molecules.

Although liquid water might properly be described as a random, three-dimensional, hydrogen-bond network,⁽²³⁾ it surely cannot have invariant fourfold coordination. Instead, some of the hydrogen bonds must be broken and others severely strained in length and direction. Nevertheless, a significant fraction of the molecules (in cold water especially) should be four-coordinated, though possibly with somewhat distorted hydrogen bonds.

In a rough way, we can think of the free liquid surface at low temperature as having been formed by passing a mathematical surface through the bulk

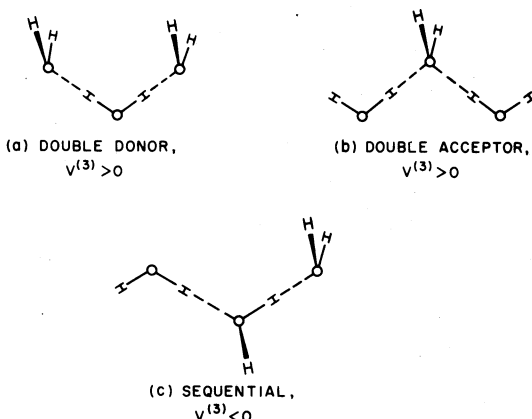


Fig. 4. The three distinct types of water-molecule trimers, involving two linear hydrogen bonds (dotted lines). These all occur in hydrogen-bond networks with fourfold tetrahedral coordination. The sign of the potential nonadditive component, $V^{(3)}$, is shown for each.

liquid, snipping all bonds that cross the surface, and then separating the two halves of the bulk phase. Figure 5 shows two water molecules that become residents of the outermost surface layer after the cutting and separation process. Both were four-coordinated to begin with, and both have two of the hydrogen bonds snipped.

One can readily count how many trimers of each type "belonging to" the resultant surface molecule have been disrupted by formation of the surface. Figure 5 shows the counts for its two examples. In view of the $V^{(3)}$ signs shown in Fig. 4, it is clearly more costly in energy, other things being equal, to cut apart configuration 5(b) than 5(a). Accordingly, we would expect to find doubly coordinated surface molecules of type 5(a) energetically preferred in a real surface over those of type 5(b).

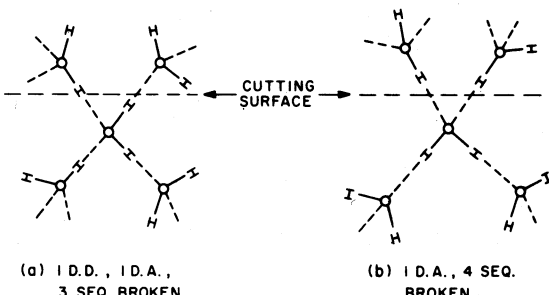


Fig. 5. Two types of four-coordinated water molecules which become two-coordinated surface-layer molecules. The "cutting surface" is the mathematical surface at which bonds are snipped to produce fresh liquid surfaces. The numbers of trimers of each type disrupted by surface formation are shown for the two initial configurations.

A configuration conjugate to 5(b) should also be considered, having both protons pointing upward across the cutting surface to neighbors above it. After cutting and separation, these protons would point out of the underlying liquid and, of course, be unbonded. We know from preceding considerations of electrical asymmetry for the molecules that this third configuration "5(c)" is itself energetically less favorable even than 5(b). We note here for completeness that "5(c)" would require breakage of one double donor trimer and four sequential trimers, so surface molecules of type 5(a) are still the preferred species on the basis of $V^{(3)}$ discrimination.

It is not possible to identify a similar energy bias, based on $V^{(3)}$ signs, which operates on surface molecules that either were less than four-coordinated to begin with, or that had one or three hydrogen bonds snipped during surface preparation. Nevertheless $V^{(3)}$ is substantial in magnitude relative to kT at room temperature,⁽¹⁵⁾ and the argument just posed is apparently relevant to a significant fraction of the molecules. Therefore, this phenomenon ought to comprise a major interfacial orienting effect whose presence should be acknowledged both in scaled-particle theories of water and in study of the free liquid surface. One must keep in mind, for the remainder of this paper, that the measurable surface tension γ_{lv} is numerically affected by this non-additivity phenomenon.

4. REVISED G FOR WATER

We now undertake to improve the calculation of $G(\lambda)$ for the rigid-sphere solute in pure water. Both the liquid-vapor surface tension and the radial distribution function for pure water will be used as input data. We shall continue to set $a = 2.75 \text{ \AA}$ to be consistent with the preceding length scale, though no direct structural significance will now be implied by that choice.

The most accurate determination to date of the oxygen-oxygen pair correlation functions $g^{(2)}(r)$ in liquid water has been carried out by Narten and Levy.^(24,6) Their results show that virtually no pairs of oxygen nuclei occur closer than 2.40 \AA (at least below 100°C). Therefore, the last expression in (5) will be correct for $G(\lambda)$ in the range $0 < \lambda < 0.4364$. For larger λ , at least the pair term in $P(\lambda)$, Eq. (4), should contribute, and so the same would be true of $G(\lambda)$.

In ice, the strong and directional forces between neighbor molecules produce characteristic isosceles triangles of oxygen nuclei, as illustrated in Fig. 6(a). The apex angle is, of course, the tetrahedral angle $\theta_t = 109^\circ 28'$; since the hydrogen bonds in ice have length 2.76 \AA , the smallest sphere which could enclose these isosceles triangles would have radius $\lambda a = 2.25 \text{ \AA}$. For ice then, nothing beyond the pair ($n = 2$) terms in $P(\lambda)$ and $G(\lambda)$ would be

⁶ The author is grateful to Dr. Narten for supplying a numerical tabulation of the function $g^{(2)}(r)$, which has been used in the present paper.

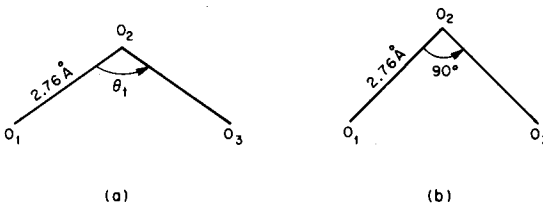


Fig. 6. Triads of oxygen nuclei. In (a) the arrangement shown corresponds to bonded neighbors in ice, with $\theta_1 = 109^\circ 28'$. The distorted triad (b) is used to estimate the radius of the smallest sphere which could reasonably be expected to circumscribe triads in the cold liquid.

required, provided that λa did not exceed 2.25 Å or, equivalently, that λ did not exceed 0.8182.

The hydrogen-bond pattern present in ice surely undergoes major distortion upon melting. Still, the coordination number in the liquid remains low, and it seems abundantly clear that the tendency toward tetrahedral bonding is a dominant feature in the liquid.⁽²⁵⁾ Consequently, it seems to be a reasonable assumption for cold liquid water that triads of oxygen nuclei are seldom distorted into a more compact arrangement than would result from reduction of θ_1 to 90°. The correspondingly distorted configuration, shown in Fig. 6(b), will now just fit into a sphere with radius

$$\lambda a = 1.95 \text{ \AA} \quad (23)$$

which occurs at $\lambda = 0.7091$. Although some oxygen-nucleus triads in the liquid may have apex angles less than 90°, it seems likely that the necessarily weakened bonds will increase in length, thereby still obeying the estimate (23).

In order to specify $G(\lambda)$ beyond the limit (23) explicitly in terms of molecular correlation functions, knowledge of $g^{(3)}$, $g^{(4)}$, ... would be required. That knowledge, of course, is unavailable.⁷ Instead, we can rely on the conventional Laurent series format for $G(\lambda)$, Eq. (8), suitably truncated. The continuity and differentiability of $G(\lambda)$ at point (23) subsequently can be used to fix unknown parameters.

The summary for $G(\lambda)$ thus is the following:

$$G(\lambda) = [1 - (4\pi/3)\rho a^3 \lambda^3]^{-1} \quad (0 < \lambda a < 1.20 \text{ \AA})$$

$$G(\lambda) = \frac{1 + (\pi\rho a^3/\lambda) \int_0^{2\lambda} dt g^{(2)}(t) t^2(t-2\lambda)}{1 - (4\pi/3)\rho a^3 \lambda^3 + (\pi\rho a^3)^2 \int_0^{2\lambda} dt g^{(2)}(t) t^2(\frac{1}{3}t^3 - 2\lambda^2 t + \frac{8}{3}\lambda^3)} \quad (1.20 \text{ \AA} < \lambda a < 1.95 \text{ \AA})$$

$$G(\lambda) = (p/\rho kT) + (2\gamma_{tv}/\rho a kT\lambda) + (G_2/\lambda^2) + (G_4/\lambda^4) \quad (1.95 \text{ \AA} < \lambda a < \infty) \quad (24)$$

⁷ For simple liquids, the Kirkwood superposition approximation might suffice to estimate $g^{(3)}, g^{(4)}, \dots$ in terms of $g^{(2)}$. That approximation is likely to be very poor for liquid water, however, and will be avoided here.

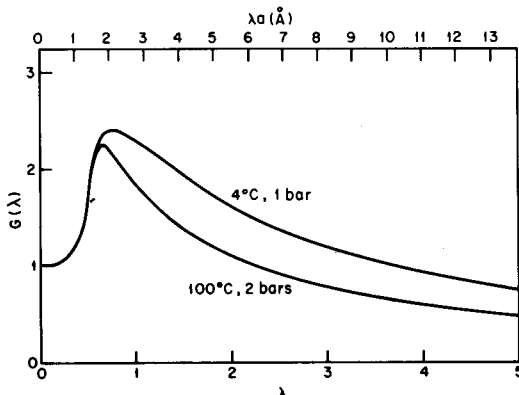


Fig. 7. Contact correlation function $G(\lambda)$ calculated according to the method of Sec. 4.

The second of these functional forms results after carrying out the $n=2$ integration in Eq. (4) and then using Eqs. (1) and (3) to yield the explicit G expression. The λ^{-3} term is missing in the last of the three forms in (24), as required by the general theory,⁷ so that $W(\lambda)$ will be free of contributions proportional to $\ln \lambda$. The quantities G_2 and G_4 are adjustable parameters whose values effect smooth connection at $\lambda a = 1.95 \text{ \AA}$.

The function $G(\lambda)$ has been calculated according to this procedure for the two sets of conditions: (1) 4°C, 1 bar; and (2) 100°C, 2 bars.⁸ The results are displayed in Fig. 7. After comparing these curves with that in Fig. 1, we see that the present more accurate procedure tends to give $G(\lambda)$ substantially larger maxima (though at roughly the same λ value) than the Pierotti hard-sphere approximation. Furthermore, the Pierotti approximation is far less sensitive to temperature (it depends essentially on the number density alone, which is nearly constant) than the more detailed result.

5. CONCLUSIONS

The fact that the revised $G(\lambda)$ calculation leads to larger maxima is relatively easy to understand. Unlike the Pierotti hard-sphere approximation, it accounts explicitly for the strong and directional hydrogen-bonding forces in water, not only through the pair correlation function $g^{(2)}$ that it utilizes but also in the selection of the λ range toward which triplets first contribute. As the exclusion sphere S_λ expands, it is forced to stretch and tear the hydrogen-bond network in its neighborhood. While this process occurs, the remaining hydrogen bonds probably reach around S_λ in a tightly drawn net, which surely enhances G .

⁸ The slight overpressures are invoked to prevent the vapor film from widening as $\lambda \rightarrow \infty$, as discussed in Sec. 3. If this measure were not adopted, the asymptotic development (8) for $G(\lambda)$ would contain terms that were not merely integer powers of λ .

At 4°C, the $G(\lambda)$ maximum shown in Fig. 7 has the value

$$G(\lambda_{\max}) = 2.3959$$

$$a\lambda_{\max} = 2.1075 \text{ \AA} \quad (25)$$

The inward stress, or "pressure," exerted by the water molecules at the surface of S_λ subsequently may be evaluated:

$$p_{\max} = \rho k T G(\lambda_{\max})$$

$$= 3.0657 \text{ kbar} \quad (26)$$

This presumably measures the extent of network stretch.

Next, we can use the general expression (14) [in the special case shown in (16)], to reveal some information about solvation of S_λ at the maximal size λ_{\max} . It seems reasonable to suppose that the contact-pair correlation function $G^{(2)}$ is simply proportional to $g^{(2)}$ at the appropriate straight-line distance:

$$G^{(2)}(\lambda, \lambda, \theta) \cong A_0 [G(\lambda)]^2 g^{(2)}[r(\lambda, \theta)] \quad (27)$$

where

$$r(\lambda, \theta) = a\lambda[1 - \cos \theta]^{1/2} \quad (28)$$

By substituting this approximation for $G^{(2)}$ into Eq. (16), a unique determination of the multiplier A_0 results:

$$\begin{aligned} A_0 &= 2 \left\{ \int_0^\pi d\theta \sin \theta (1 - \cos \theta) g^{(2)}[r(\lambda_{\max}, \theta)] \right\}^{-1} \\ &= 4a^4 \lambda_{\max}^4 \left\{ \int_0^{2a\lambda_{\max}} dr r^3 g^{(2)}(r) \right\}^{-1} \end{aligned} \quad (29)$$

The value implied by Eq. (29) for A at 4°C is

$$A_0 = 1.048 \quad (30)$$

Figure 8 shows a plot of the resulting function $G^{(2)}(\lambda_{\max}, \lambda_{\max}, \theta)$ vs angle. Similar curves could be obtained for $\lambda \neq \lambda_{\max}$ from Eq. (14), but the results would be trivial for small λ ; the results would furthermore be unreliable at large λ because estimate (27) would then become inappropriate.

It is important to reflect upon the local solvent structures which might contribute to the function $G^{(2)}(\lambda, \lambda, \theta)$. To be sure, a wide variety of hydrogen-bond network fragments must be present in liquid water,⁽²³⁾ but statistically they seem to present important common features. Figure 9 shows a specific example of the way that the network can surround S_λ when the size parameter is approximately λ_{\max} . This particular cage consists of 12 water molecules arranged into four pentagons and two hexagons. Only the oxygen positions

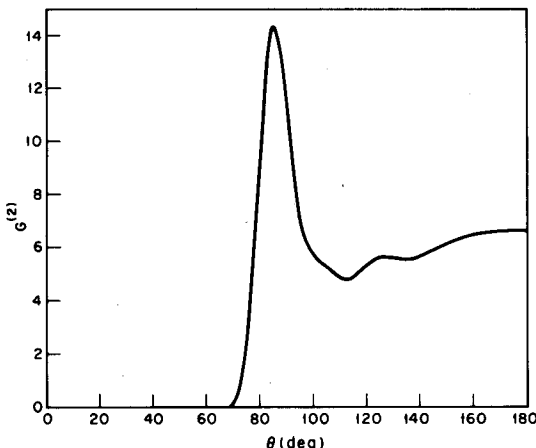


Fig. 8. Surface-pair correlation function $G^{(2)}(\lambda_{\max}, \lambda_{\max}, \theta)$ for water at 4°C and 1 bar. Figure 2 provides the relevant geometry, with $\lambda a = 2.1075 \text{ \AA}$.

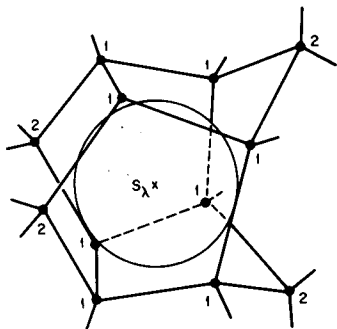


Fig. 9. "Random" water-molecule cage enclosing the rigid-sphere solute, whose exclusion sphere is denoted by S_λ . The oxygen nuclei are shown as dark circles, and hydrogen bonds as dark lines. Protons can be distributed asymmetrically along the bonds in a variety of canonical ways. Oxygen nuclei "1" are closer to the solute than those of type "2."

are explicitly shown (as dark circles). The protons can be assigned to the hydrogen bonds (dark lines) in a variety of ways that is analogous to the variety underlying the configurational disorder in ice.⁽²⁶⁾

Notice that the eight water molecules nearest to the center of S_λ , which have been indicated by "1" in the figure, are all oriented so that one of the four tetrahedral bond directions points radially outward, i.e., away from the center of S_λ . For each of these eight, then, the remaining three bond directions straddle S_λ . As a result, the dipole-moment direction for these solvent molecules cannot point either toward, or directly away from, the hard-sphere solute. The four more remote solvent molecules denoted by "2" in Fig. 9, however, can point their dipole-moment vectors either inward or outward along the radial direction.

Model building shows that this orientational bias for nearest-neighbor solvent molecules is very marked and extends to S_λ radii well in excess of $a\lambda_{\max} \approx 2.1 \text{ \AA}$. Evidently the geometric requirement that the nearest solvents form a predominately convex solvation "cage" forces them to adopt the straddling mode. The cages present in aqueous clathrates⁽²⁷⁾ exhibit precisely

this characteristic too, though they represent only a small fraction of the total possible cage geometries. Probably the largest convex cage that could reasonably be expected to form on energetic grounds would be the one whose bonds have the pattern displayed by soccer balls: Sixty water molecules form 12 pentagons and 20 hexagons, and each of these molecules straddles the cavity interior.⁹

The water molecule bonding situation depicted in Fig. 9 is unrealistic in that no severely stretched, twisted, or broken hydrogen bonds are shown. The true situation is therefore more complicated, but the orientational bias just adduced for first-layer solvent molecules must still be a substantial phenomenon since extensive hydrogen bonding exists. For the statistical tendency to be present, of course, we need not demand that the random solvation cages be perfectly bonded. In any event, the orientational bias certainly becomes less pronounced as temperature increases.

The situation which leads to the small-cavity solvation effects on water molecule orientation is not relevant to large λ . When λa exceeds the range 3–4 Å, the processes leading to formation of the free liquid surface (at low pressure) described in Sec. 3 would probably dominate. One should keep in mind, however, that many interesting solutes have sizes below this range, so that convex cage statistics is indeed relevant to their solutions.

As a useful "thought experiment," we can imagine placing electrostatic charge uniformly on our hard-sphere solute particle to convert it into a monatomic ion. The strong electric fields that result would have the effect of twisting first-layer solvation molecules out of "straddling" configurations into those with radial directions for dipole moments. This structural rearrangement likely plays an important role in the thermodynamics of ionic solvation.⁽²⁸⁾

It would be very desirable to augment the conclusions in this paper with independent evidence. The molecular-dynamics technique has recently been adapted to the study of pure water.⁽²⁹⁾ In principle, it could be modified to incorporate rigid-sphere solutes of arbitrary size. Not only would this permit the $G(\lambda)$ curves in Fig. 7 to be checked quantitatively, but the geometry of solvation cages could also be observed. It would then be interesting to see if the approximation, on which the function $G^{(2)}$ shown in Fig. 8 was calculated, was in fact accurate. In the long run, there is hope that the combination of such stylistically independent procedures could lead to understanding solvation subtleties such as hydrophobic bonding in the biochemical regime.⁽³⁰⁾

ACKNOWLEDGMENT

The author has enjoyed a protracted and constructive dialogue with Professor Henry S. Frank on the nature of water and aqueous solutions. This

⁹ Assuming that the hydrogen bonds forming this maximal cage have length 2.8 Å, its radius would be about 6.4 Å.

interaction has helped the former to maintain in his work a respectable balance between the sterile intricacy of formal theory and the seductive simplicity of poetic "explanation."

REFERENCES

1. H. Reiss, H. L. Frisch, and J. L. Lebowitz, *J. Chem. Phys.* **31**, 369 (1959).
2. E. Helfand, H. L. Frisch, and J. L. Lebowitz, *J. Chem. Phys.* **34**, 1037 (1961).
3. E. Helfand, H. Reiss, and H. L. Frisch, *J. Chem. Phys.* **33**, 1379 (1960).
4. H. Reiss, *Advan. Chem. Phys.* **IX**, 1-84 (1965).
5. D. M. Tully-Smith and H. Reiss, *J. Chem. Phys.* **53**, 4015 (1970).
6. H. Reiss and D. M. Tully-Smith, *J. Chem. Phys.* **55**, 1674 (1971).
7. F. H. Stillinger and M. A. Cotter, *J. Chem. Phys.* **55**, 3449 (1971).
8. M. A. Cotter and F. H. Stillinger, *J. Chem. Phys.* **57**, 3356 (1972).
9. H. Reiss, *Advan. Chem. Phys.* **IX**, 78 (1965), Table XVI.
10. H. Reiss, H. L. Frisch, E. Helfand, and J. L. Lebowitz, *J. Chem. Phys.* **32**, 119 (1960).
11. R. A. Pierotti, *J. Phys. Chem.* **69**, 281 (1965).
12. K. Morokuma and L. Pederson, *J. Chem. Phys.* **48**, 3275 (1968).
13. P. A. Kollman and L. C. Allen, *J. Chem. Phys.* **51**, 3286 (1969).
14. J. Del Bene and J. A. Pople, *J. Chem. Phys.* **52**, 4858 (1970).
15. D. Hankins, J. W. Moskowitz, and F. H. Stillinger, *J. Chem. Phys.* **53**, 4544 (1970).
16. G. H. F. Diercksen, *Theoret. Chim. Acta (Berlin)* **21**, 335 (1971).
17. A. H. Narten and H. A. Levy, *J. Chem. Phys.* **55**, 2263 (1971).
18. F. P. Buff, *J. Chem. Phys.* **19**, 1591 (1951).
19. M. Losonczy, J. W. Moskowitz, and F. H. Stillinger, to be published.
20. B. Widom, *J. Chem. Phys.* **43**, 3892 (1965).
21. K. Kinosita and H. Yokota, *J. Phys. Soc. Japan* **20**, 1086 (1965).
22. F. H. Stillinger and A. Ben-Naim, *J. Chem. Phys.* **47**, 4431 (1967).
23. J. D. Bernal, *Proc. Roy. Soc. (London)* **A280**, 299 (1964); J. D. Bernal, in *Liquids: Structure, Properties, Solid Interactions*, T. J. Hughel, ed. (Elsevier Publishing Co., New York, 1965), p. 25.
24. A. H. Narten and H. A. Levy, *J. Chem. Phys.* **55**, 2263 (1971).
25. A. H. Narten and H. A. Levy, *Science* **165**, 447 (1969).
26. L. Pauling, *J. Am. Chem. Soc.* **57**, 2680 (1935).
27. L. Pauling, *The Nature of the Chemical Bond* (Cornell University Press, Ithaca, 1960), p. 469.
28. H. S. Frank and W.-Y. Wen, *Disc. Faraday Soc.* **24**, 133 (1957).
29. A. Rahman and F. H. Stillinger, *J. Chem. Phys.* **55**, 3336 (1971); F. H. Stillinger and A. Rahman, *J. Chem. Phys.* **57**, 1281 (1972).
30. W. Kauzmann, *Advan. Protein Chem.* **14**, 1 (1959).

EDITOR'S NOTE

This paper was substituted for the talk originally given by Dr. Stillinger at the H. S. Frank Symposium. Consequently, no Discussion section is available.